MICROBIOLOGY

RESEARCH ARTICLE
Rangarajan *et al.*, *Microbiology* 2022;168:001180
DOI 10.1099/mic.0.001180

MICROBIOLOGY SOCIETY

Ruminococcus bromii enables the growth of proximal *Bacteroides thetaiotaomicron* by releasing glucose during starch degradation

Aathmaja Anandhi Rangarajan[1], Hannah E. Chia[2], Christopher A. Azaldegui[2], Monica H. Olszewski[1], Gabriel V. Pereira[3], Nicole M. Koropatkin[3] and Julie S. Biteen[1,2,*]

Abstract

Complex carbohydrates shape the gut microbiota, and the collective fermentation of resistant starch by gut microbes positively affects human health through enhanced butyrate production. The keystone species *Ruminococcus bromii* (*Rb*) is a specialist in degrading resistant starch; its degradation products are used by other bacteria including *Bacteroides thetaiotaomicron* (*Bt*). We analysed the metabolic and spatial relationships between *Rb* and *Bt* during potato starch degradation and found that *Bt* utilizes glucose that is released from *Rb* upon degradation of resistant potato starch and soluble potato amylopectin. Additionally, we found that *Rb* produces a halo of glucose around it when grown on solid media containing potato amylopectin and that *Bt* cells deficient for growth on potato amylopectin (Δ*sus Bt*) can grow within the halo. Furthermore, when these Δ*sus Bt* cells grow within this glucose halo, they have an elongated cell morphology. This long-cell phenotype depends on the glucose concentration in the solid media: longer *Bt* cells are formed at higher glucose concentrations. Together, our results indicate that starch degradation by *Rb* cross-feeds other bacteria in the surrounding region by releasing glucose. Our results also elucidate the adaptive morphology of *Bt* cells under different nutrient and physiological conditions.

INTRODUCTION

The human gut microbiome consists of trillions of microbes, most belonging to the phyla *Firmicutes* and *Bacteroidetes* [1, 2]. The health benefits provided to the host by a well-balanced gut microbiota include digestion of complex polysaccharides, synthesis of micronutrients, resistance against pathogens and development of immunity [3, 4]. The microbial composition varies across different regions of the gut and this composition is highly organized into distinct biogeographies depending on nutrient availability [5–9]. The formation of these coexisting bacterial communities results from an intricate synergy between members of the gut microbiome during carbohydrate breakdown [10–12]. For example, mucin cross-feeding has been reported between infant *Bifidobacteria* and *Eubacterium hallii* [13]. *Bifidobacterium pseudolongum* degrades Hi-Maize-resistant starch whose byproducts are used by other bifidobacterial species [14]. Cross-feeding has also been observed in *Bifidobacterium longum, Anaerostipes caccae* and *Roseburia intestinalis* during growth on oligofructose [15]. However, there exists a fundamental gap in our knowledge about the metabolic and spatial relationships between gut microbiome members during cross-feeding at the single-cell level.

Diet is a major factor that influences the gut microbiota, and it can cause short- and long-term changes in gut microbial communities [16–18]. Starch is the most abundant polysaccharide in the Western diet [19]. Resistant starch is indigestible by humans but can be utilized by the microbiota; this metabolism creates short chain fatty acids (SCFAs) such as butyrate, which confer enormous health benefits to the host [20–24]. The firmicute *Ruminococcus bromii* (*Rb*) has evolved a unique extracellular multiprotein enzymatic machinery known as the amylosome. Akin to cellulosome complexes synthesized by cellulose-degrading bacteria and fungi, amylosomes comprise dockerin-containing enzymes that bind cohesin domains on scaffoldin proteins, and this protein complex efficiently binds and degrades resistant starch [25–28]. *Rb* is one of the few gut bacteria that can degrade

Received 05 February 2022; Accepted 01 April 2022; Published 26 April 2022
Author affiliations: [1]Department of Chemistry, University of Michigan, Ann Arbor, Michigan, USA; [2]Program in Chemical Biology, University of Michigan, Ann Arbor, Michigan, USA; [3]Department of Microbiology and Immunology, University of Michigan Medical School, Ann Arbor, Michigan, USA.
***Correspondence:** Julie S. Biteen, jsbiteen@umich.edu
Keywords: gut microbiome; *Ruminococcus*; *Bacteroides*; starch; cross-feeding; microscopy.
Abbreviations: *Bt*, *Bacteroides thetaiotaomicron*; GOPOD, glucose oxidase/peroxidase; HPAEC-PAD, high-performance anion exchange chromatography with pulsed amperometric detection; NMR, nuclear magnetic resonance; OD, optical density; PUL, polysaccharide utilization locus; *Rb*, *Ruminococcus bromii*; RUM, Ruminococcus medium; SCFA, short chain fatty acid; SEM, standard error of the mean; *sus*, starch utlization system.
Nine supplementary figures are available with the online version of this article.

Impact Statement

Dietary intake of complex carbohydrates including resistant starch benefits human health by supporting the growth of keystone species that increase the microbiome diversity via cross-feeding. For instance, *Ruminococcus bromii* (*Rb*) is a specialist in degrading resistant starch, and the byproducts of this degradation process are used by bacterial species. In this study, we show that *Bacteroides thetaiotaomicron* (*Bt*) cross-feeds on the glucose released during potato starch degradation by *Rb*. We also show that proximity to *Rb* cells that are releasing sugars is important for growth of the cross-fed *Bt* in solid media. Additionally, we find a longer phenotype for *Bt* cells grown on solid media in high glucose conditions, indicating that, like other bacteria, human gut bacteria undergo significant nutrient-dependent morphological adaptations.

resistant starch, and thus it acts as a 'keystone' species that supports other species by releasing sugars and other metabolites [25, 26, 29, 30]. *Bacteroides thetaiotaomicron (Bt)* is another prominent member of the gut microbiome, but unlike *Rb*, *Bt* cannot break down resistant starch. However, *Bt* does have the ability to catabolize several types of glycans, including various types of monosaccharides, oligosaccharides and soluble polysaccharides. Specific oligo- or polysaccharides induce the expression of discrete polysaccharide utilization loci (PULs) genes, which are otherwise silent, to enable the digestion and utilization of specific polysaccharides [31–33]. Though *Bt* can utilize a wide variety of dietary or host-derived glycans, the availability of a specific carbon source to *Bt* is shaped by the local gut environment [6, 34]. When grown in co-culture with *Rb*, *Bt* can cross-feed on the resistant corn starch degradation products of *Rb*. However, the metabolic profile of the sugars that *Rb* provides to *Bt* during potato starch degradation is unknown. Though most previous studies of cross-feeding between gut microbes have been performed in liquid media, bacteria in the gut are in fact confined to the solid intestinal surface [8, 9, 13–15, 25]. It is therefore imperative to visualize and quantify the cross-feeding between *Rb* and *Bt* on a solid surface to understand how the number of bacteria, the distance between cells and their surface tethering affect this interaction.

The spatial properties of a microbial community also depend strongly on the environment. Bacteria possess unique cell morphologies that help them survive in their native environments [35]. For instance, large bacteria are typically found in nutrient-rich environments such as insect guts and marine sediments [36]. Several bacterial species, including gut bacteria, change their size and shape to adapt to various nutrient and environmental conditions [37–39]. These pleomorphic bacteria regulate their cellular machinery to form longer phenotypes to survive in response to a physiological or environmental change. Uropathogenic *Escherichia coli*, *Legionella pneumophila* and *Streptococcus pneumoniae* form long filaments to evade the host immune response and enhance attachment to host cell surfaces [40–42]. Other bacteria such as *Proteus mirabilis* and *Vibrio parahaemolyticus* sense solid surfaces through flagella and elongate to promote swarming motility [43, 44]. How gut anaerobes adapt to different nutrient and environmental conditions at the single-cell and community level has not been well studied [39].

The ability of *Rb* to degrade resistant corn starch and soluble starch and cross-feed other bacteria including *Bt* has been described [25, 29]. However, we lack a detailed understanding of the metabolic and spatial relationships between *Rb* and other bacteria that support this cross-feeding. In this study, we show that *Rb* releases glucose as the major byproduct of the degradation of both resistant potato starch and soluble potato amylopectin. Furthermore, we show that *Bt* growth on solid media is enhanced near *Rb* that is releasing the byproducts of potato amylopectin degradation. Moreover, with microscopy we show that cross-fed *Bt* has a longer phenotype in proximity to *Rb* when compared to *Bt* that is distant from *Rb* due to the local prevalence of released glucose. This model system we have constructed on solid media provides a lens into bacterial cross-feeding in the gut environment.

METHODS

Bacterial strains and growth conditions

Δsus UnaG Bt, which fluoresces in the presence of bilirubin [45], was generated by counter-selectable allelic exchange in a *ΔsusA-G Bt* (*Δtdk*) thymidine kinase deletion mutant with codon-optimized UnaG cloned under a constitutive promoter, and grown as previously described [46]. *Bt* ATCC 29148 (VPI-5482) and its derivative *Δsus UnaG Bt* were grown in TYG medium [47] or minimal medium [48]. Bilirubin was added in the media to a final concentration of 25 µM. Carbon sources were added to 5 mg ml^{-1} unless otherwise stated. *Rb* L2-63 was grown in modified RUM medium [26], consisting of (per 100 ml) tryptone (0.5 g), yeast extract (0.25 g), resazurin (50 µg), haematin (30 µM), L-histidine (3 mM), a salt mixture consisting of $NaHCO_3$ (0.4 g), L-cysteine (0.1 g), $(NH_4)_2SO_4$ (0.09 g), K_2HPO_4 (0.045 g), KH_2PO_4 (0.045 g), NaCl (0.09 g), $MgSO_4$ (0.004 g) and $CaCl_2$ (0.009 g), and a vitamin mixture consisting of biotin (20 µg), cobalamin (20 µg), *p*-aminobenzoic acid (60 µg), folic acid (100 µg), pyridoxamine (300 µg), thiamine (100 µg), riboflavin (100 µg), D-pantothenoic acid hemicalcium salt (100 µg) and nicotinamide (100 µg). An SCFA mixture consisting of acetic acid (63.7 mM), propionic acid (17.8 mM), isobutyric acid (5.75 mM), isovaleric acid (1.95 mM) and valeric acid (1.95 mM) was also added. The pH was set to 7.4±0.2 using 6 M NaOH. The medium was filter sterilized and reduced in the anaerobic chamber before inoculation. 2×RUM medium was diluted with

an equal volume of a carbohydrate solution containing maltose (final concentration 5 mg ml^{-1}), fructose (final concentration 5 mg ml^{-1}) and glycogen (final concentration 2.5 mg ml^{-1}) or potato amylopectin (final concentration 5 mg ml^{-1}) to grow the cells. Resistant potato starch (Bob's Red Mill raw potato starch, unmodified) was sterilized with 70% ethanol twice and air dried before use (final concentration 25 mg ml^{-1}). All strains were grown at 37 °C under anaerobic conditions (5% H_2, 85% N_2, 10% CO_2) in an anaerobic chamber. The OD_{600} was measured using a spectrophotometer (Genesys 20; Thermo Fisher Scientific) or absorbance reader (PowerWave HT; Biotek Instruments). Data were recorded using Gen5 software (BioTek Instruments) and Prism (GraphPad).

Growth of bacteria in solid media

A modified RUM medium was used for growing *Rb* and *Bt* in solid media. For 100 ml media, 95 ml of water was mixed with tryptone (0.5 g), agarose (2 g) and the salt mixture as described in the previous section except $NaHCO_3$ and autoclaved. After autoclaving this medium, a filter sterilized solution consisting of $NaHCO_3$, L-cysteine, resazurin, haematin, L-histidine, the vitamin mixture and the SCFA mixture were added in the final concentration as described in the previous section. The pH was set to 8±0.2 using 6 M NaOH. Potato amylopectin was used at 5 mg ml^{-1} for growing *Rb*. For growing *Bt,* glucose, ribose, xylose or maltose was used at 200 µM, 2 mM or 20 mM final concentration, respectively. Potato amylopectin was used at final concentration of 0.4, 2, or 10 mg ml^{-1}. The plates were reduced for 48 h inside the anaerobic chamber. *Rb* cells were washed with modified RUM media without carbon source and *Bt* cells were washed with minimal media without carbon source before plating. Then, 10 µl of *Rb* and *Bt* cells were plated and incubated for 72 h before taking the plate pictures and determining the glucose concentration. After 24 h of incubation, in plates previously inoculated with *Rb* at the centre, *Bt* was plated at different distances from *Rb* (0.5, 1, 1.5 and 2 cm) and incubated for 72 h before taking plate pictures (Color QCount; Spiral Biotech).

Determination of glucose concentration in agarose plates

For determination of glucose in the RUM media plates, 1 cm^2 samples were cut from the agar, dissolved in a 2× volume of 6 M sodium iodide and heated at 55 °C for 15 min. The dissolved agarose solution was used to determine the concentration of glucose according to the manufacturer's instructions (D-Glucose assay kit, GOPOD format; Megazyme).

Isolation of spent RUM media

Rb was inoculated in modified RUM media with resistant potato starch (final concentration 25 mg ml^{-1}) or potato amylopectin (final concentration 5 mg ml^{-1}) as a carbon source. After 72 h of growth, the samples were centrifuged at 5000 r.p.m. for 5 min. The supernatant spent RUM was removed and filter sterilized with a 0.2 µm filter. To this spent RUM, 1×RUM salt mixture solution mentioned above was added to achieve a pH of 7 before inoculating with *Bt*.

Analysis of sugars using high-performance anion exchange chromatography with pulsed amperometric detection (HPAEC-PAD)

HPAEC-PAD analysis of soluble sugars was done using the ICS-6000 system (Thermo Scientific Dionex). Samples were separated with a CarboPac PA-100 anion exchange column (250×2 mm; Thermo Fisher Scientific) and a CarboPac PA-100 guard column (Thermo Fisher Scientific). Detection was enabled by PAD with a gold working electrode and an Ag/AgCl reference electrode using a standard AAA potential waveform for mono- and oligosaccharides and a quadruple potential waveform for polysaccharides. Each sample was run on the column for 40 min at a constant flow rate of 1 ml min^{-1}. A gradient composed of the following eluents was used at 25 °C: (buffer A) 0.1 M sodium hydroxide, (buffer B) 0.1 M sodium hydroxide +0.5 M sodium acetate. Before every run, the column was washed with 100% buffer A for 10 min. For monosaccharides and oligosaccharides, the following gradient was applied after injection: 0–5 min, isocratic 100% buffer A; 5–24 min, linear gradient to 50% buffer A and 50% buffer B; 24–34 min, 100% buffer B. For polysaccharides, the following gradient was applied after injection: 0–60 min, linear gradient to 90% buffer B and 10% A; 61–74 min, 90% buffer A and 10% buffer B. We used 1 mM glucose, maltose, maltotriose and maltotetraose, and 5 mg ml^{-1} potato amylopectin as standards. For the standard calibration curves, 3, 1.5, 0.75, 0.375 and 0.187 mM glucose standards were used. Data integration and analysis were performed using the Chromeleon 7.2 chromatography data system (Thermo Scientific Dionex).

Sample preparation and live-cell imaging

Samples were placed on gridded coverslip (28 mM, 50 µm grids; IBIDI) and sealed with epoxy (5 min Epoxy; Devcon) to maintain cells under anaerobic conditions and to enable live-cell imaging [49]. Phase-contrast images were taken on an Olympus IX71 inverted fluorescence microscope using a 1.40 numerical aperture 100× wide-field oil-immersion objective. *UnaG Bt* and *Δsus UnaG Bt* cell samples were imaged using a 488 nm laser (Coherent Sapphire 488–50; 8–18 W cm^{-2}) with a 488 nm long pass filter, and fluorescence emission was detected on a 512×512 pixel Photometrics Evolve electron-multiplying charge-coupled device camera at 25 frames s^{-1}.

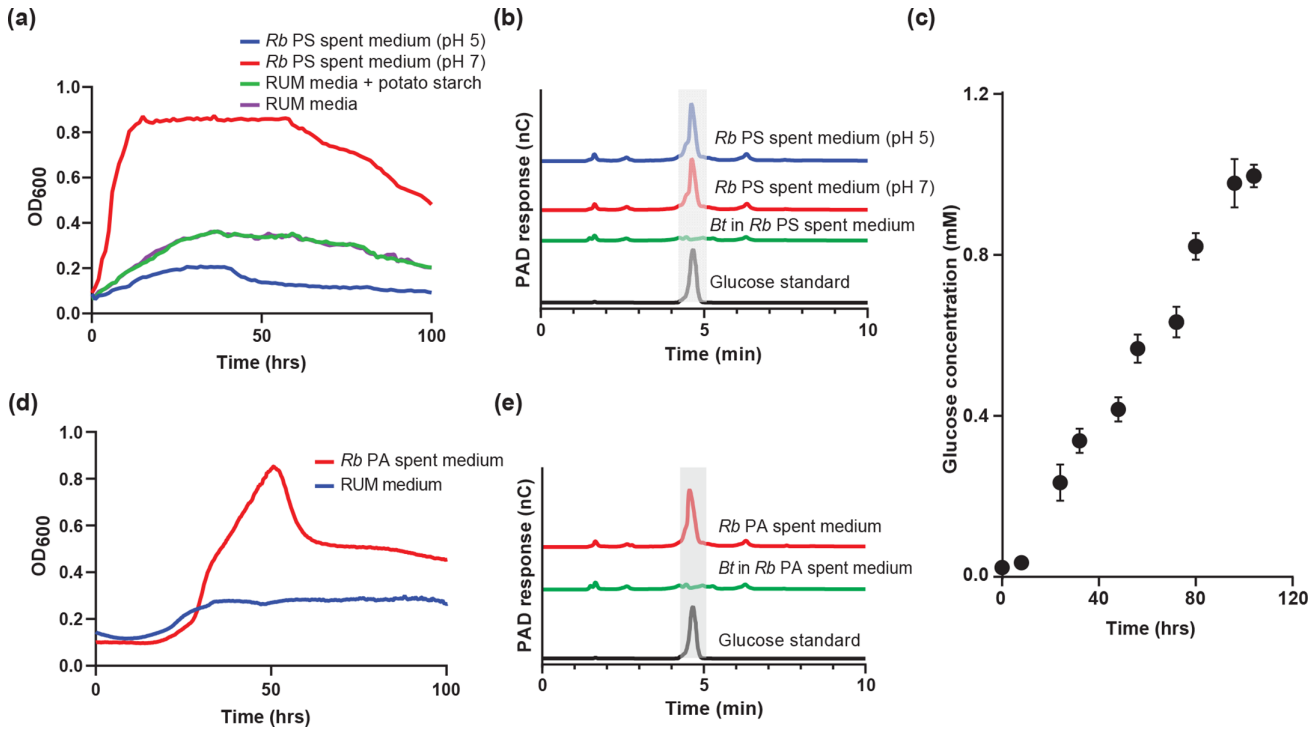

Fig. 1. (a) Growth of *Bt* cells in *Rb* resistant potato starch (PS) spent medium (pH 5, blue), neutralized *Rb* potato starch spent medium (pH 7, red), RUM medium with resistant potato starch (green) and RUM medium alone (magenta) measured by absorbance at 600 nm. Mean values of three biological replicates are shown. (b) Analysis of the spent medium by HPAEC-PAD. The shaded grey region on the traces highlights where the glucose peak would be if glucose is present. Black, blue, red and green traces represent the glucose standard, *Rb* resistant potato starch spent medium at pH 5, *Rb* resistant potato starch spent medium at pH 7 and *Rb* resistant potato starch spent medium at pH 7 after growth of *Bt* cells, respectively. (c) Glucose concentration in *Rb* resistant potato starch spent medium isolated at different time points (0–104 h). Three biological replicates were used for this HPAEC-PAD analysis. Error bars indicate SEM. (d) Growth of *Δsus unaG Bt* cells in neutralized *Rb* spent medium isolated from *Rb* cells grown in potato amylopectin (PA, red) and RUM medium control (blue) measured by absorbance at 600 nm. (e) Analysis by HPAEC-PAD of the *Rb* spent medium isolated from *Rb* cells grown in potato amylopectin. The shaded grey region on the traces highlights where the glucose peak would be if glucose is present. Black, red and green traces represent the glucose standard, *Rb* potato amylopectin spent medium and *Rb* potato amylopectin spent medium after growth of *Δsus unaG Bt* cells, respectively.

Cell length measurements

Cell segmentation and quantification of cell dimensions were done with a custom Python script. Phase masks were produced using an in-house trained cell segmentation model implemented with Cellpose [50]. Erroneous segmentations were manually corrected using the Cellpose graphical user interface. Cell lengths and widths were determined from the long and short axis of each cell in the phase mask using the scikit-image Python package [51]. Mean lengths and widths were calculated and *P*-values were determined using one-way ANOVA and post-hoc Tukey tests with 95% confidence intervals.

RESULTS

The major byproduct of resistant potato starch degradation by *Rb* is glucose, which is then utilized by *Bt*

We investigated the ability of *Bt* to cross-feed on the byproducts of resistant potato starch degradation by *Rb* based on previous studies that showed that *Bt* can grow on the products of resistant corn degradation by *Rb* in co-culture [25]. While *Rb* can grow on starch and malto-oligosaccharides, most strains including the *Rb* L2-63 used in our study cannot grow on glucose [27]. We isolated the spent medium after *Rb* growth on resistant potato starch by filtering out the *Rb* cells. Growth of *Rb* on resistant starch acidifies the medium, which was initially at pH 7.4±0.2, to pH 5 after 72 h of growth (Fig. S1a). Despite the presence of cross-feeding sugars from *Rb*, the low pH inhibits *Bt* growth consistent with previous findings (Fig. S1b) [52]. However, after it is neutralized to pH 7, *Bt* can grow in the spent medium of *Rb* with no additional carbohydrate source due to the presence of the sugars released by *Rb* (Fig. 1a). We identified the sugars released by *Rb* with HPAEC-PAD, which showed that glucose is the major byproduct of the resistant starch degradation of potato starch by *Rb*. This glucose is utilized by *Bt* during growth in the neutralized spent medium after 24 h of growth (Fig. 1b). Next, we quantified the amount of glucose released as *Rb* grows in resistant potato starch. The glucose concentration increases with time as *Rb* degrades resistant potato starch and reaches ~1 mM

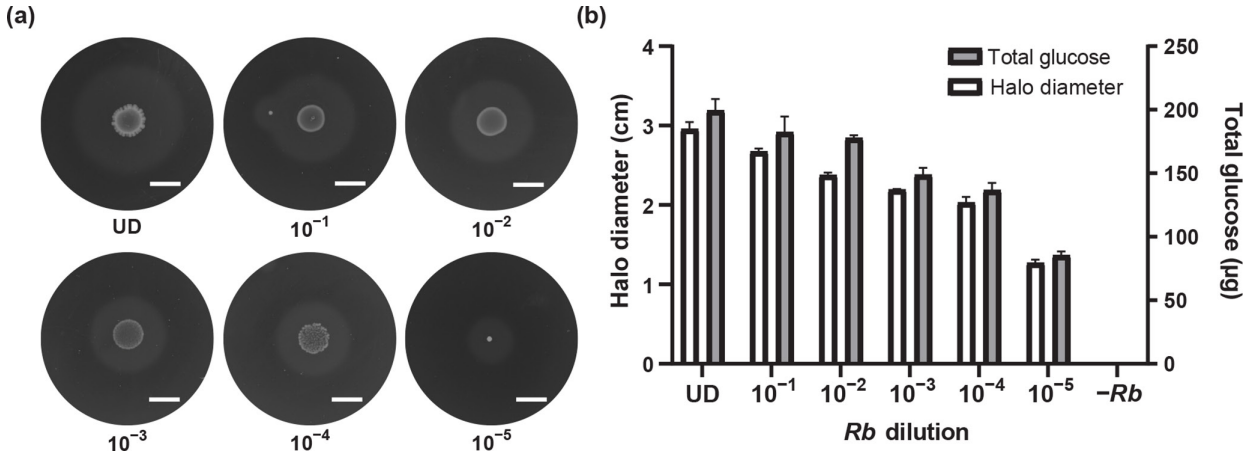

Fig. 2. (a) Pictures of *Rb* cells plated on agarose plates at dilutions from undiluted (UD) to 10^{-5} with potato amylopectin (5 mg ml^{-1}) showing a halo around the cells. Scale bars, 1 cm. (b) Halo diameter (white bars) and total mass of glucose in the halo (grey bars) for each *Rb* dilution. The average values of two biological replicates are shown. Error bars indicate SEM.

after 96 h (Figs 1c and S2a). No maltose, malto-oligosaccharides or soluble polysaccharides were identified in our analysis; if generated, these may be rapidly utilized by *Rb* instead of glucose (Fig. S2b, c). These results show that *Rb* releases glucose as the major byproduct of resistant potato starch degradation, that the amount of glucose in the medium increases over time and that this glucose is utilized by *Bt*.

Spatial proximity to the glucose released by *Rb* on potato amylopectin agarose helps Δ*sus UnaG Bt* growth

Gut bacteria are confined to spatially distinct regions of the intestine and can be tethered to the solid intestinal surface [6, 8]. To study the cross-feeding between *Rb* and *Bt* in a spatial context, we used solid agarose plates with potato amylopectin as a carbon source, since the cloudiness of the insoluble resistant starch makes cells grown on this source unsuitable for microscopy analysis. *Rb* grows on potato amylopectin similar to growth on fructose and glycogen as the carbon source (Fig. S3a). Since *Bt* can also grow on amylopectin, we used a *Δsus Bt* strain in which the *sus* operon (*susA-G*) is deleted, and tagged it with the anaerobic fluorescent protein UnaG, which fluoresces in the presence of a bilirubin cofactor when excited at 488 nm [45]. The constructed *Δsus UnaG Bt* strain cannot grow on potato amylopectin but can grow on glucose and fluoresces in the presence of a bilirubin cofactor when excited at 488 nm (Fig. S3b, c). This *Δsus UnaG Bt* strain can also grow on the neutralized spent medium of *Rb* grown in potato amylopectin (Fig. 1d). HPAEC-PAD showed that *Rb* releases glucose after utilizing potato amylopectin similar to resistant potato starch, and that this glucose is utilized by *Bt* (Fig. 1e). As in liquid cultures, we confirmed that *Rb* can grow on agarose plates supplemented with amylopectin whereas *Δsus UnaG Bt* cannot (Fig. S4). Moreover, *Rb* growing on potato amylopectin plates form a 'halo' of glucose (Fig. 2a). Though the concentration of glucose (amount per cm^2) remains constant across different dilutions of *Rb* (Fig. S5), the halo diameter and thus the total amount of glucose detected decrease with *Rb* dilution (Fig. 2b).

Next, we spotted *Δsus UnaG Bt* at different distances (0.5–2 cm) from *Rb* to study the effect of their spatial proximity to *Rb*. Across different dilutions, we measured *Δsus UnaG Bt* growth from the absorbance intensity, which is proportional to the colony density. *Δsus UnaG Bt* grew better within the halo of glucose released by *Rb* relative to *Δsus UnaG Bt* outside the halo (Fig. 3a–c). The percentage area of the *Bt* colony inside the halo linearly correlates with the intensity of the colony observed across all dilutions (Fig. 3d). These results show that spatial proximity to *Rb* releasing glucose results in better growth of *Δsus UnaG Bt* due the local availability of glucose released by *Rb*.

Single-cell analysis reveals a longer Δ*sus UnaG Bt* phenotype near *Rb* releasing glucose on solid media

To analyse the cell morphology of *Δsus UnaG Bt* cells inside and outside the halo, we imaged the cells at 0 and 6 h using the gridded coverslip as a reference for unbiased sampling. We previously reported an elongated phenotype (2.3 µm) for *Bt* cells grown in liquid medium under sugar-limited conditions in the presence of sodium carbonate [39]. Hence, we hypothesized that *Δsus UnaG Bt* cells grown within the glucose halo of *Rb* would have the wild-type phenotype, while *Δsus UnaG Bt* in the sugar-limited region outside the halo would have the elongated phenotype. However, contrary to our expectations, *Δsus UnaG Bt* grown inside the halo containing glucose had a longer phenotype (2.4 µm) compared to the cells outside the halo (1.9 µm) after 6 h of incubation (Figs 4a, b and S6a). The longer cells inside the halo are similar to the *Δsus UnaG Bt* cells plated on glucose (125 µM) in terms of size and density (Figs 4a, b and S6b). On the other hand, *Δsus UnaG Bt* cells grown in liquid medium with glucose (27 mM), the

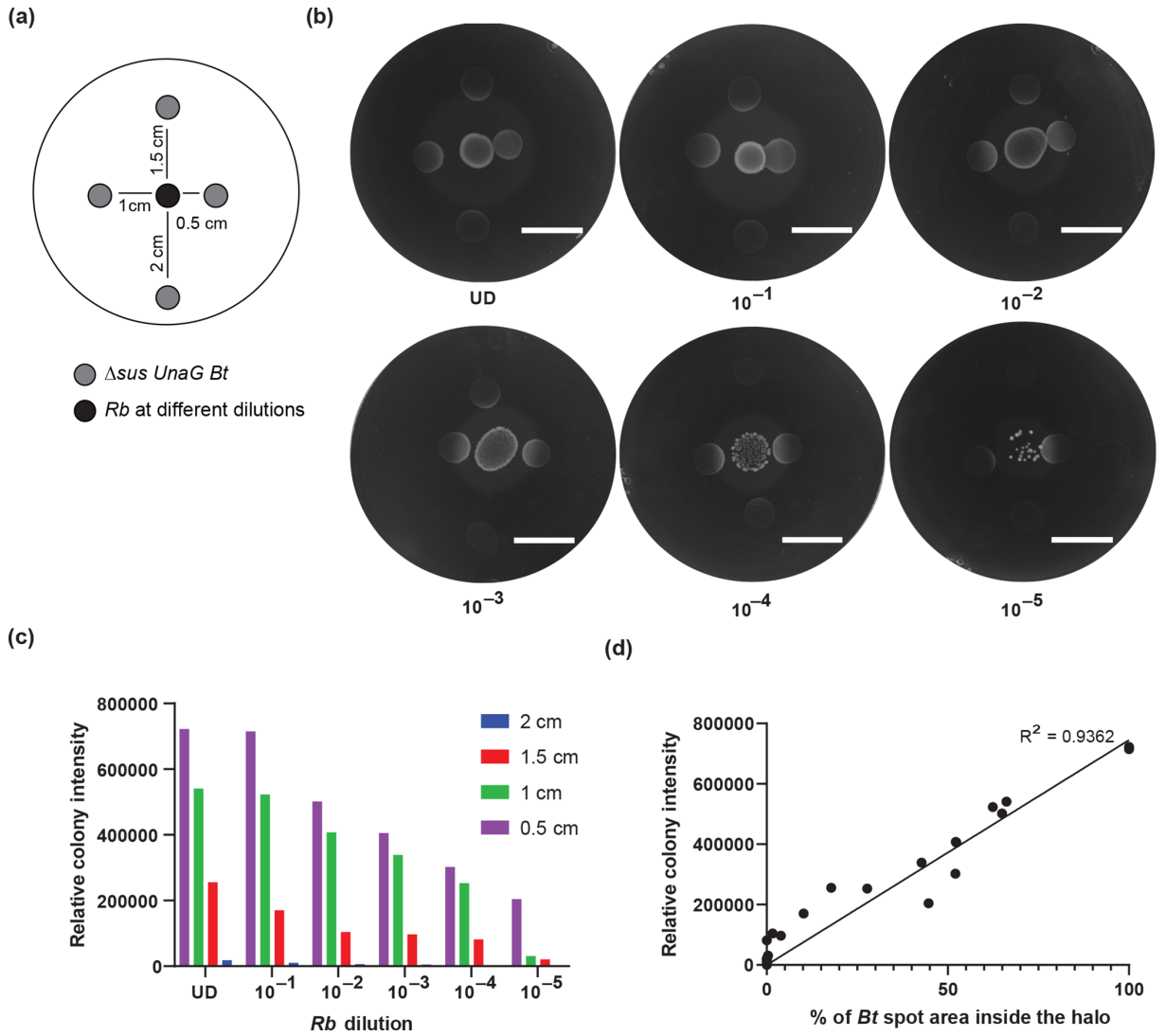

Fig. 3. (a) Schematic of the potato amylopectin plates prepared to analyse the spatial relationship between *Δsus UnaG Bt* and *Rb*: 10 µl *Δsus UnaG Bt* was spotted at four different distances from a central spot of *Rb*. (b) Pictures of cells plated on agarose plates with potato amylopectin (5 mg ml^{-1}). The central *Rb* cells were plated at dilutions from undiluted (UD) to 10^{-5} and a grey halo was observed around this spot. *Δsus UnaG Bt* cells were spotted at 0.5, 1, 1.5 and 2 cm from the *Rb*. Scale bars, 2 cm. (c) Growth of each *Bt* spot measured as the intensity of the spot relative to the background intensity. (d) We calculated the percentage area inside the halo for each *Δsus UnaG Bt* spot and compared it to the normalized intensity of that *Δsus UnaG Bt* spot. Data points corresponding to all *Rb* dilutions and all distances of *Δsus UnaG Bt* are represented as dots. Black line: fit to a linear curve.

concentration typically used for growing *Bt*, showed no difference in length after 6 h of incubation (Fig. S7). These results show that *Δsus UnaG Bt* cells grown on solid media have a longer morphology in the vicinity of *Rb* releasing glucose.

The longer *Bt* morphology in solid media depends on the glucose concentration

To test whether this longer morphology is specific to glucose alone or a general phenomenon, we analysed the morphology of wild-type *Bt* cells grown on solid media with other monosaccharides (xylose or ribose), the disaccharide maltose or the polysaccharide potato amylopectin. *Bt* uses a unique set of genes to transport and metabolize each of these sugars [34, 53–55]. Wild-type *Bt* cells were plated on solid media with different concentrations of sugar (200 µM, 2 mM or 20 mM) and on potato amylopectin (0.4, 2 or 10 mg ml^{-1}) and imaged after 6 h of incubation. In glucose, the cell length was 1.8 µm at the time of incubation (0 h), which increased to 2.2 µm at 200 µM after 6 h of incubation (Fig. 4c, d). The average length was even higher (3.5 µm) after incubation in 2 mM glucose, and incubation at 20 mM produced very long cells (average length of 6.9 µm with some cells as long as 27 µm) (Figs 4c, d and S8). In all the mono- and disaccharides tested, the cells at 20 mM sugar concentration were significantly elongated relative to cells at 200 µM sugar concentration (Fig. S9a–c). A similar increase in cell size was seen for

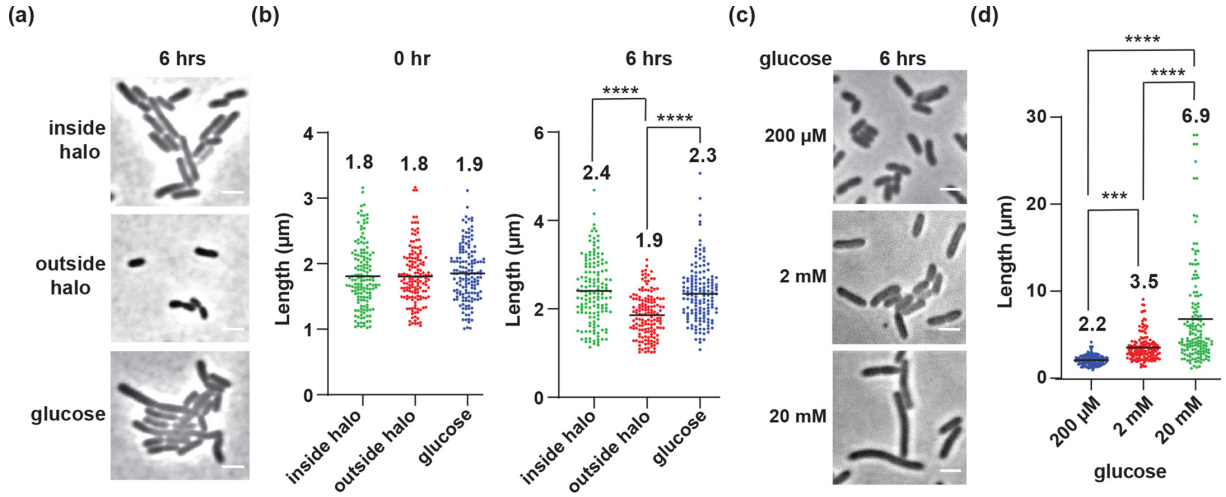

Fig. 4. (a) Representative phase-contrast micrographs of *Δsus UnaG Bt* cells inside the glucose halo, outside the glucose halo and on plates with glucose at 6 h. Scale bars, 2 µm. (b) Length of *Δsus UnaG Bt* cells grown inside the glucose halo (green), outside the glucose halo (red), and on plates with glucose (blue) at 0 and 6 h. Each circle represents the length of a single cell from a set of three biological replicates (n=150 cells). Mean value is indicated by a black line. Statistical significance was determined by one-way ANOVA and post-hoc Tukey tests. Significant differences are indicated by asterisks (****P<0.0001) (c) Representative phase-contrast micrographs of wild-type *Bt* cells taken after 6 h of incubation on plates with 200 µM, 2 mM and 20 mM glucose. Scale bars, 2 µm. (d) Length of wild-type *Bt* cells grown on 200 µM (blue), 2 mM (red) and 20 mM (green) glucose for 6 h. Each circle represents the length of a single cell from a set of three biological replicates (n=150 cells). Statistical significance was determined by one-way ANOVA and post-hoc Tukey tests. Significant differences are indicated by asterisks (****P<0.0001, ***P<0.001).

cells grown with amylopectin at 10 mg ml^{-1} (2.2 µm) compared to 0.4 mg ml^{-1} (1.9 µm) (Fig. S9d). However, contrary to what was observed with glucose, we did not see a consistent increase in cell length as a function of concentration for xylose, ribose and potato amylopectin. At 20 mM, the very long *Bt* cells seen with glucose were seen only for few outliers in maltose and were never seen at similar concentrations of xylose, ribose or potato amylopectin (Fig. S9). These results show that *Bt* adapts its morphology at higher concentrations of different sugars in solid media, but that the concentration-dependent increase in cell size, including very long cells at 20 mM, is seen only in glucose.

DISCUSSION

Rb has evolved to possess specialized proteins that form amylosome complexes that efficiently bind and degrade resistant starches, and *Rb* has been established as a keystone species in the gut microbiota because it produces starch degradation byproducts that cross-feed other community members [25–29]. Studying the mechanism of this metabolism and resource sharing will provide important information toward understanding community formation and maintenance. In this study, we show that *Rb* releases glucose upon degradation of resistant starch and soluble potato amylopectin (Fig. 1). On a solid surface, the glucose released in the vicinity of *Rb* can be utilized by *Bt* (Fig. 3). Our results complement recent findings which showed that *Rb* possesses several surface-anchored and secreted amylosome complex proteins with starch-binding and starch-degrading capacity [26, 27]. These proteins can bind and degrade starch in our system to produce the glucose byproduct that we observe as a halo of glucose around *Rb* (Figs 2a and 3b). The total glucose amount and the halo diameter decreased with higher dilutions of *Rb* (Figs 2 and 3b). This decrease in total glucose at higher *Rb* dilutions is probably due to there being less amylosome complex present when the *Rb* cell density is lower. This degradation outside the *Rb* cell can help other proximal bacteria, such as *Bt*, allowing them to utilize these byproducts and thrive in the complex gut environment. Further studies are needed to elucidate the mechanism and dynamics of resistant starch degradation.

In our study, HPAEC-PAD analysis of the products of resistant potato starch degradation by *Rb* showed that glucose is the only major byproduct; we did not identify any other oligosaccharides or polysaccharides (Fig. S2b, c). A previous study of the degradation of Hi-Maize-resistant starch by *Rb* by NMR spectroscopy detected minor amounts of maltose and maltotetraose in addition to glucose [29]. This difference may be due to differences between potato starch and Hi-Maize substrates or differences in sensitivity between HPAEC-PAD and NMR. However, the absence of anything but glucose in our assays indicates that *Rb* immediately utilizes any oligomeric byproducts as they are released. Alternatively, because the *Rb* amylosome complex contains several dockerin-containing proteins that are capable of binding longer and shorter oligosaccharides [26–28], it is also plausible that any oligosaccharides byproducts that form from resistant starch degradation are bound by dockerin proteins and filtered out of the spent medium.

Morphological pleomorphism and plasticity have been observed in several bacterial species in response to a variety of nutrient and environmental conditions [56]. We previously observed elongated *Bt* cells (2.3 µm) in nutrient-poor conditions in liquid medium in the presence of sodium carbonate [39]. However, contrary to our expectations, when *Bt* was grown on solid media, we observes an elongated phenotype at higher sugar concentrations; this result was consistent across a variety of sugars: glucose, maltose, xylose, ribose and potato amylopectin polysaccharide (Figs 4d and S9). This effect was more pronounced in glucose: the *Bt* cell size increased with glucose concentration, and very long *Bt* cells (mean length 6.9 µm) grew at the highest glucose concentration of 20 mM (Fig. 4c, d). This result indicates that the *Bt* cell elongation machinery might be regulated by glucose, similar to observations in *E. coli* and *B. subtilis* in which the cell elongation machinery is regulated by uridine diphosphate glucose through FtsZ [36, 57, 58]. The solid surface affects the *Bt* cell elongation machinery, similar to other bacteria which form long filamentous structures upon attachment to a solid surface [40, 41, 43, 44]. We observed a differential regulation of the cell division machinery for *Bt* in solid and liquid media under different nutrient conditions. The underlying molecular mechanisms involved in the differential phenotypic responses to nutrient availability under varied nutrient and environmental conditions require further investigation. The adaptation of *Bt* to various nutrient conditions both in liquid medium and on solid surfaces may allow this bacterium to effectively compete with other bacteria and persist within the gut ecosystem.

Funding information
This work was supported by Army Research Office grant W911NF-18-1-0339 to J.S.B. and N.M.K.

Acknowledgements
We thank Eric C. Martens for access to the BioTek plate reader and Dionex ICS-6000 system. We also thank Supriya Suresh Kumar for construction of the Δ*susA-G* mutant. We are grateful to the Mobley lab for access to their Colour QCount.

Author contributions
A.A.R., H.E.C., N.M.K. and J.S.B. conceived the study and designed the experiments. A.A.R. conducted all the experiments. G.V.P. and M.H.O. assisted in HPAEC-PAD analysis and method development. C.A.A. curated and analysed cell length measurements. A.A.R. and J.S.B. wrote the manuscript. All authors revised the final version of the manuscript.

Conflicts of interest
The authors declare that there are no conflicts of interest.

References

1. Qin J, Li R, Raes J, Arumugam M, Burgdorf KS, *et al*. A human gut microbial gene catalogue established by metagenomic sequencing. *Nature* 2010;464:59–65.
2. D'Argenio V, Salvatore F. The role of the gut microbiome in the healthy adult status. *Clin Chim Acta* 2015;451:97–102.
3. Kho ZY, Lal SK. The human gut microbiome - a potential controller of wellness and disease. *Front Microbiol* 2018;9:1–23.
4. McCarville JL, Chen GY, Cuevas VD, Troha K, Ayres JS. Microbiota metabolites in health and disease. *Annu Rev Immunol* 2020;38:147–170.
5. Koropatkin NM, Cameron EA, Martens EC. How glycan metabolism shapes the human gut microbiota. *Nat Rev Microbiol* 2012;10:323–335.
6. Tropini C, Earle KA, Huang KC, Sonnenburg JL. The gut microbiome: connecting spatial organization to function. *Cell Host Microbe* 2017;21:433–442.
7. Donaldson GP, Lee SM, Mazmanian SK. Gut biogeography of the bacterial microbiota. *Nat Rev Microbiol* 2016;14:20–32.
8. Sheth RU, Li M, Jiang W, Sims PA, Leong KW, *et al*. Spatial metagenomic characterization of microbial biogeography in the gut. *Nat Biotechnol* 2019;37:877–883.
9. Whitaker WR, Shepherd ES, Sonnenburg JL. Tunable expression tools enable single-cell strain distinction in the gut microbiome. *Cell* 2017;169:538–546.
10. Rakoff-Nahoum S, Coyne MJ, Comstock LE. An ecological network of polysaccharide utilization among human intestinal symbionts. *Curr Biol* 2014;24:40–49.
11. Rakoff-Nahoum S, Foster KR, Comstock LE. The evolution of cooperation within the gut microbiota. *Nature* 2016;533:255–259.
12. Hoek MJA van, Merks RMH. Emergence of microbial diversity due to cross-feeding interactions in a spatial model of gut microbial metabolism. *BMC Syst Biol* 2017;11:1–18.
13. Bunesova V, Lacroix C, Schwab C. Mucin cross-feeding of infant bifidobacteria and *Eubacterium hallii*. *Microb Ecol* 2018;75:228–238.
14. Centanni M, Lawley B, Butts CA, Roy NC, Lee J, *et al*. *Bifidobacterium pseudolongum* in the ceca of rats fed hi-maize starch has characteristics of a keystone species in bifidobacterial blooms. *Appl Environ Microbiol* 2018;84:1–11.
15. Falony G, Vlachou A, Verbrugghe K, De Vuyst L. Cross-feeding between *Bifidobacterium longum* BB536 and acetate-converting, butyrate-producing colon bacteria during growth on oligofructose. *Appl Environ Microbiol* 2006;72:7835–7841.
16. David LA, Maurice CF, Carmody RN, Gootenberg DB, Button JE, *et al*. Diet rapidly and reproducibly alters the human gut microbiome. *Nature* 2014;505:559–563.
17. Sonnenburg ED, Smits SA, Tikhonov M, Higginbottom SK, Wingreen NS, *et al*. Diet-induced extinctions in the gut microbiota compound over generations. *Nature* 2016;529:212–215.
18. Flint HJ, Duncan SH, Louis P. The impact of nutrition on intestinal bacterial communities. *Curr Opin Microbiol* 2017;38:59–65.
19. Cordain L, Eaton SB, Sebastian A, Mann N, Lindeberg S, *et al*. Origins and evolution of the Western diet: health implications for the 21st century. *Am J Clin Nutr* 2005;81:341–354.
20. Morrison DJ, Preston T. Formation of short chain fatty acids by the gut microbiota and their impact on human metabolism. *Gut Microbes* 2016;7:189–200.
21. Baxter NT, Schmidt AW, Venkataraman A, Kim KS, Waldron C, *et al*. Dynamics of human gut microbiota and short-chain fatty acids in response to dietary interventions with three fermentable fibers. *mBio* 2019;10:1–13.
22. Dalile B, Van Oudenhove L, Vervliet B, Verbeke K. The role of short-chain fatty acids in microbiota-gut-brain communication. *Nat Rev Gastroenterol Hepatol* 2019;16:461–478.
23. Klingbeil EA, Cawthon C, Kirkland R, de La Serre CB. Potato-resistant starch supplementation improves microbiota dysbiosis,

inflammation, and gut-brain signaling in high fat-fed rats. *Nutrients* 2019;11:11.

24. DeMartino P, Cockburn DW. Resistant starch: impact on the gut microbiome and health. *Curr Opin Biotechnol* 2020;61:66–71.
25. Ze X, Duncan SH, Louis P, Flint HJ. *Ruminococcus bromii* is a keystone species for the degradation of resistant starch in the human colon. *ISME J* 2012;6:1535–1543.
26. Ze X, Ben David Y, Laverde-Gomez JA, Dassa B, Sheridan PO, *et al*. Unique organization of extracellular amylases into amylosomes in the resistant starch-utilizing human colonic firmicutes bacterium *Ruminococcus bromii*. *mBio* 2015;6:e01058-15.
27. Mukhopadhya I, Moraïs S, Laverde-Gomez J, Sheridan PO, Walker AW, *et al*. Sporulation capability and amylosome conservation among diverse human colonic and rumen isolates of the keystone starch-degrader *Ruminococcus bromii*. *Environ Microbiol* 2018;20:324–336.
28. Cerqueira FM, Photenhauer AL, Pollet RM, Brown HA, Koropatkin NM. Starch digestion by gut bacteria: crowdsourcing for carbs. *Trends Microbiol* 2020;28:95–108.
29. Crost EH, Le Gall G, Laverde-Gomez JA, Mukhopadhya I, Flint HJ, *et al*. Mechanistic insights into the cross-feeding of *Ruminococcus gnavus* and *Ruminococcus bromii* on host and dietary carbohydrates. *Front Microbiol* 2018;9:1–13.
30. Laverde Gomez JA, Mukhopadhya I, Duncan SH, Louis P, Shaw S, *et al*. Formate cross-feeding and cooperative metabolic interactions revealed by transcriptomics in co-cultures of acetogenic and amylolytic human colonic bacteria. *Environ Microbiol* 2019;21:259–271.
31. Tancula E, Feldhaus MJ, Bedzyk LA, Salyers AA. Location and characterization of genes involved in binding of starch to the surface of *Bacteroides thetaiotaomicron*. *J Bacteriol* 1992;174:5609–5616.
32. Lapébie P, Lombard V, Drula E, Terrapon N, Henrissat B. Bacteroidetes use thousands of enzyme combinations to break down glycans. *Nat Commun* 2019;10:2043.
33. Ndeh D, Gilbert HJ. Biochemistry of complex glycan depolymerisation by the human gut microbiota. *FEMS Microbiol Rev* 2018;42:146–164.
34. Glowacki RWP, Pudlo NA, Tuncil Y, Luis AS, Sajjakulnukit P, *et al*. A ribose-scavenging system confers colonization fitness on the human gut symbiont *Bacteroides thetaiotaomicron* in a diet-specific manner. *Cell Host Microbe* 2020;27:79–92.
35. Young KD. Bacterial morphology: why have different shapes? *Curr Opin Microbiol* 2007;10:596–600.
36. Levin PA, Angert ER. Small but mighty: cell size and bacteria. *Cold Spring Harb Perspect Biol* 2015;7:a019216.
37. Yang DC, Blair KM, Salama NR. Staying in shape: the impact of cell shape on bacterial survival in diverse environments. *Microbiol Mol Biol Rev* 2016;80:187–203.
38. Kysela DT, Randich AM, Caccamo PD, Brun YV. Diversity takes shape: understanding the mechanistic and adaptive basis of bacterial morphology. *PLoS Biol* 2016;14:1–15.
39. Rangarajan AA, Koropatkin NM, Biteen JS. Nutrient-dependent morphological variability of *Bacteroides thetaiotaomicron Microbiology (Reading)* 2020;166:624–628.
40. Mulvey MA, Schilling JD, Hultgren SJ. Establishment of a persistent *Escherichia coli* reservoir during the acute phase of a bladder infection. *Infect Immun* 2001;69:4572–4579.
41. Prashar A, Bhatia S, Tabatabaeiyazdi Z, Duncan C, Garduño RA, *et al*. Mechanism of invasion of lung epithelial cells by filamentous *Legionella pneumophila*. *Cell Microbiol* 2012;14:1632–1655.
42. Rodriguez JL, Dalia AB, Weiser JN. Increased chain length promotes pneumococcal adherence and colonization. *Infect Immun* 2012;80:3454–3459.
43. Gode-Potratz CJ, Kustusch RJ, Breheny PJ, Weiss DS, McCarter LL. Surface sensing in *Vibrio parahaemolyticus* triggers a programme of gene expression that promotes colonization and virulence. *Mol Microbiol* 2011;79:240–263.
44. Belas R, Suvanasuthi R. The ability of *Proteus mirabilis* to sense surfaces and regulate virulence gene expression involves FliL, a flagellar basal body protein. *J Bacteriol* 2005;187:6789–6803.
45. Chia HE, Zuo T, Koropatkin NM, Marsh ENG, Biteen JS. Imaging living obligate anaerobic bacteria with bilin-binding fluorescent proteins. *Curr Res Microb Sci* 2020;1:1–6.
46. Koropatkin NM, Martens EC, Gordon JI, Smith TJ. Starch catabolism by a prominent human gut symbiont is directed by the recognition of amylose helices. *Structure* 2008;16:1105–1115.
47. Holdeman LV, Moore WEC. Anaerobe Laboratory Manual; 1973 (Virginia Polytechnic Institute and State University, Blacksburg, Va. V.P.I. Anaerobe Laboratory); (n.d.). https://books.google.com/books?id=qYr9HAAACAAJ
48. Martens EC, Chiang HC, Gordon JI. Mucosal glycan foraging enhances fitness and transmission of a saccharolytic human gut bacterial symbiont. *Cell Host Microbe* 2008;4:447–457.
49. Karunatilaka KS, Cameron EA, Martens EC, Koropatkin NM, Biteen JS. Superresolution imaging captures carbohydrate utilization dynamics in human gut symbionts. *mBio* 2014;5:e02172.
50. Stringer C, Wang T, Michaelos M, Pachitariu M. Cellpose: a generalist algorithm for cellular segmentation. *Nat Methods* 2021;18:100–106.
51. van der Walt S, Schönberger JL, Nunez-Iglesias J, Boulogne F, Warner JD, *et al*. scikit-image: image processing in Python. *PeerJ* 2014;2:e453.
52. Duncan SH, Louis P, Thomson JM, Flint HJ. The role of pH in determining the species composition of the human colonic microbiota. *Environ Microbiol* 2009;11:2112–2122.
53. Foley MH, Cockburn DW, Koropatkin NM. The Sus operon: a model system for starch uptake by the human gut *Bacteroidetes*. *Cell Mol Life Sci* 2016;73:2603–2617.
54. Liu H, Shiver AL, Price MN, Carlson HK, Trotter VV, *et al*. Functional genetics of human gut commensal *Bacteroides thetaiotaomicron* reveals metabolic requirements for growth across environments. *Cell Rep* 2021;34:108789.
55. Townsend GE, Han W, Schwalm ND, Hong X, Bencivenga-Barry NA, *et al*. A master regulator of *Bacteroides thetaiotaomicron* gut colonization controls carbohydrate utilization and an alternative protein synthesis factor. *mBio* 2020;11:2020.
56. Caccamo PD, Brun YV. The molecular basis of noncanonical bacterial morphology. *Trends Microbiol* 2018;26:191–208.
57. Sargent MG. Control of cell length in *Bacillus subtilis*. *J Bacteriol* 1975;123:7–19.
58. Zaritsky A, Woldringh CL, Helmstetter CE, Grover NB. Dimensional rearrangement of *Escherichia coli* B/r cells during a nutritional shift-down. *J Gen Microbiol* 1993;139:2711–2714.

Edited by: S. P Diggle and D. J. Clarke